Original Article

In silico screening of *Andrographis paniculata* secondary metabolites as anti-diabetes mellitus through PDE9 inhibition

Netty Ino Ischak[1],*, La Ode Aman[1],*, Hamsidar Hasan[2], Akram La Kilo[1], and Aiyi Asnawi[3]

[1]*Chemistry Department, Universitas Negeri Gorontalo, Gorontalo, Indonesia.*
[2]*Pharmacy Department, Universitas Negeri Gorontalo, Gorontalo, Indonesia.*
[3]*Faculty of Pharmacy, Universitas Bhakti Kencana, Bandung, West Java, Indonesia.*

Abstract

Background and purpose: *Andrographis paniculata* (AP) has long been used as an anti-diabetic agent, but the mechanism of action and active substance responsible for the anti-diabetic effect, particularly by inhibiting phosphodiesterase-9 (PDE9), which is one of the targets of anti-diabetic medications, have not been reported. The aim of the present study was to identify a new anti-diabetes candidate from secondary metabolite compounds of AP through PDE9 inhibition.
Experimental approach: In order to prepare the chemical structures of the secondary metabolites of AP and PDE9, docking and molecular dynamics simulations were run using Discovery Studio Visualizer, AutoDockTools, AutoDock, and Gromacs, along with a few other supporting software packages.
Findings/Results: Molecular docking simulations showed that two of the 46 secondary metabolites of AP had higher free energies of binding, C00003672 (-11.35 kcal/mol) and C00041378 (-9.27 kcal/mol), than native ligand (-9.23 kcal/mol). The results of molecular dynamics showed that compound C00041378 interacted with TRY484 and PHE516, two active side residues of PDE9. ΔGMMGBSA interactions of PDE9 with C00003672, C00041378, and 49E compounds are 51.69, -56.43, and -48.13 kcal/mol, respectively, as well as ΔGMMPBSA interactions of PDE9 with C00003672, C00041378, and 49E compounds, were -12.26, -16.24, and -11.79 kcal/mol kcal/mol, respectively.
Conclusions and implications: Based on the evaluations of AP secondary metabolites using docking and molecular dynamics simulation, it is suggested that the C00041378 compound has the potential to be an anti-diabetic candidate by inhibiting PDE9.

Keywords: Andrographis paniculate; Anti-diabetic; Molecular docking; Molecular dynamics, PDE9; Secondary metabolites.

INTRODUCTION

The International Diabetes Federation (IDF) reported diabetes was responsible for 6.7 million deaths in 2021 and the number of people with diabetes mellitus (DM) in the world's population aged 20 to 79 years will reach 573 million. This means that one out of every ten people in the world was diabetic. IDF predicts that the number of people with DM will continue to increase so it is estimated that in 2030 it will reach 643 million people and in 2045 it will reach 783 million people (1).

DM is a metabolic disorder disease that causes high blood sugar levels (hyperglycaemia) for a long time, which can occur due to the inability of the pancreas to produce sufficient amounts of insulin (insulin-dependent DM), the inability of the body's cells to respond to insulin (non-insulin-dependent DM), or related to pregnancy in women who are pregnant (gestational DM).

*Corresponding authors:
L.O. Aman, Tel: +62-811404084, Fax: +62-035-821752
Email: laode_aman@ung.ac.id
N.I. Ischak, Tel: +62-81340516545, Fax: +62-035-821752
Email: netty.ischak@ung.ac.id

The failure of the pancreas to produce sufficient insulin is caused by the loss of beta cells of pancreatic islets as insulin producers, and the loss of beta cells can occur due to an autoimmune response. Non-insulin-dependent DM (called insulin resistance) is mainly caused by lifestyle and genetic factors such as obesity (body mass index greater than 30), lack of physical activity, poor diet, stress, and urbanization. Gestational diabetes resembles type 2 diabetes, in that it combines insulin secretion and low responsiveness in pregnant women that may improve after delivery (2,3).

Uncontrolled hyperglycaemia can cause various complications, such as kidney problems, eye damage, and erectile dysfunction. Insulin injections are very necessary for people with insulin-dependent DM, and for people with non-insulin-dependent DM, it could be treated by administering oral drugs such as metformin, which reduces glucose production in the liver; sulfonylureas, which increases insulin release; acarbose, which reduces sugar absorption in the intestine; sitagliptin, which inhibits the enzyme dipeptidyl peptidase-4 by inactivating incretin, thiazolidinedione, which makes the body more sensitive to insulin, as well as SGLT2 blocking drugs that increase glucose excrete (4). Although there are many anti-diabetic drugs available to control DM, research on the development of anti-diabetic drugs is still urgent, especially for cases when the available drugs are not effective, and considering genetic variations and new perspectives of treatment (5).

Natural products in the form of biodiversity, with countless secondary metabolites, are still a strategic source in the search for new drugs (6). Common anti-diabetic drugs such as metformin and biguanidine are examples of anti-diabetic agents that were developed from natural isolates, such as galegine from the plant *Galega officinalis* L. (7). The use of natural products in the ethnomedicinal communities guided by bioassays with certain pharmacological activities has become the most widely applied drug development route.

Andrographis paniculata (AP) is one of the medicinal plants used for traditional diabetes therapy by the Gorontalo community (one of the ethnic groups in Indonesia). Testing of simplicial and extracts of AP, *in vivo* and *in vitro*, showed the presence of anti-diabetic activity (8-10). AP has long been used as an anti-diabetic, but the mechanism of action and active substance responsible for the anti-diabetic effect, particularly by inhibiting phosphodiesterase-9 (PDE9), which is one of the targets of anti-diabetic medications, have not been reported (11).

PDE is a group of enzymes that break down cGMP and cAMP and has been used as a target for drugs to treat human diseases. It is well established that it plays a critical role in a variety of physiological processes, including steroid hormone function, cardiac and smooth muscle contraction, apoptosis, leukocyte migration, hyperplasia, platelet aggregation, the adrenal glands, axon regulation and regeneration, inflammation, circadian regulation, and memory. More than 100 protein isoforms are encoded by the human PDE genes, which are divided into 11 families. cGMP is a specific substrate for PDE5, PDE6, and PDE9, and cAMP is a specific substrate for PDE4, PDE7, and PDE8. In addition to cGMP and cAMP, there are several other PDE families that can inhibit them (12,13).

Several studies targeting the cGMP signaling pathway in the treatment of DM through PDE inhibition such as PDE3 inhibition able to increase insulin action, PDE3B inhibition able to mediate lipolysis inhibition by proinsulin C-peptide adipose tissue in diabetic rats, PDE5 inhibition able to increases insulin response to glucose and muscle microvascular blood flow and increases insulin resistance. It has been demonstrated that inhibiting PDE10A protects mice from diet-induced obesity and insulin resistance (14). Several PDE9 inhibitors have been patented as anti-diabetic, including BAY73-6691 a selective inhibitor of PDE9, and PF-04447943, and PF-4181366 are very strong inhibitors of PDE9A (15).

The *in-silico* method has become the front-runner to improve the speed and accuracy of the process of discovering new drugs because of its capacity to speed up the process of identification and optimization of lead compounds. By looking at how the ligand and

target interact, techniques like molecular docking and molecular dynamics (MD) were able to directly point to a small number of compounds with high affinity and selectivity (16). This work assessed the potential of AP secondary metabolites as anti-diabetic agents *via* PDE9 inhibition by investigating the stability interactions of secondary metabolite compounds with PDE9 using docking and MD simulations with the free energy of binding calculations using the molecular mechanics generalized born and surface area (MMGBSA) or ΔGMMGBSA and the molecular mechanics Poisson-Boltzmann and surface area (MMPBSA) or ΔGMMPBSA.
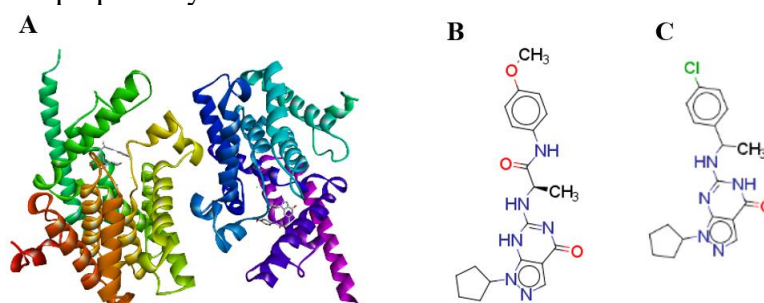
MATERIALS AND METHODS

Software

Molecular docking simulation using Autodock (17), MD simulation using the GROMACS 2021.3 program package (18), with some supporting software such as Acpype (19), UCSF Chimera (20), MODELLER (21), and the antechamber package of Ambertools 2021 (22). Chemical structure visualization using Discovery Studio Visualizer (23) and MarvinSketch (24). AutoDockTools 1.5.6 version (17) is used for molecular docking preparation and data analysis. Analysis of MD results using gmx_MMPBSA and gmx_MMPBSA_ana (25).

Protein preparation

The protein data bank (PDB) ID of the PDE9 enzyme is 4Y87. The protein exists in a complex with 49E compounds as an inhibitor of PDE9 (26). Another inhibitor compound of PDE9 is 35O (27). The complex of PDE9 and both inhibitors are shown in Fig. 1.

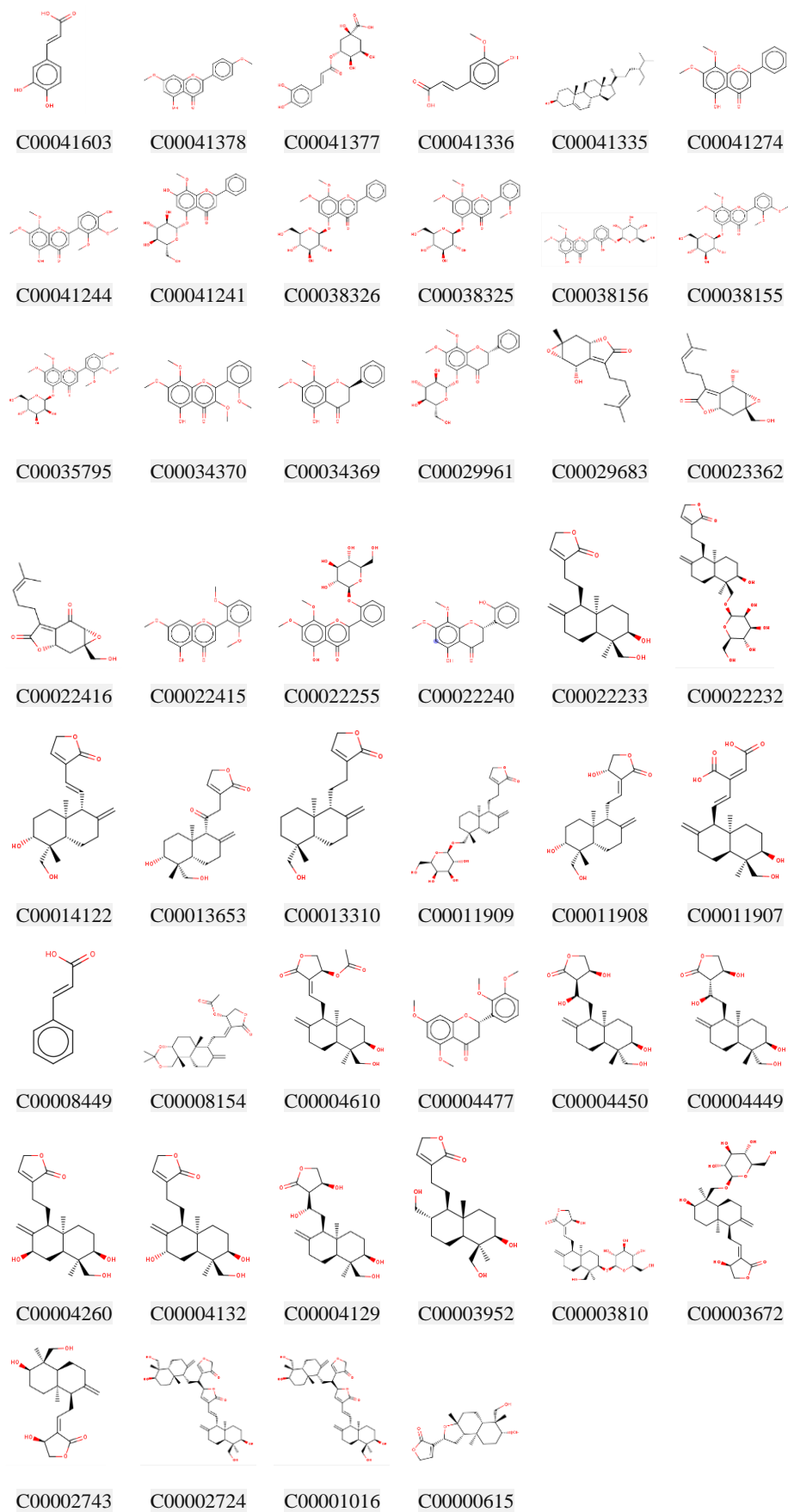The 4Y87 was downloaded from the PDB web server (28). The preparatory action is required for removing water molecules and other atoms or molecules and selecting chain A as the object of research. The next step is to separate the structures of the protein and native ligand. Protein structures for docking and MD studies were prepared by fixing break residues using the MODELLER module integrated into the Chimera. Atomic repair, hydrogen addition, and protein loading were carried out using AutoDockTools.

Ligands preparation

The database of natural products provided by the Maebashi Institute of Technology and Nara Institute of Science and Technology (29) shows AP contains 46 secondary metabolites. The three-dimensional structure of each compound is shown in Fig. 2. The determination of the rotatable bond of each native and test ligand was done by default setting, *i.e.,* all bonds that allow rotation are activated as rotatable bonds.

Molecular docking simulation

The active site of PDE9 was validated by applying the re-docking protocol of a native ligand. By comparing the coordinates of the native ligand in its crystal structure with PDE9 and after redocking, the root mean square distance (RMSD) of both positions is obtained. A validated active site is when the RMSD value is less than or equal to 2 Å (30). The docking process of the test ligand compounds to PDE9 was carried out on the validated active site. The whole molecular docking process (for both the native and test ligands) was done using autodock with the help of AutoDockTools to prepare based on the same criteria: protein rigidity, genetic algorithm parameter with GA runs of 20, and a maximum number of energy evaluations of 25,000,000 on the number of rotatable bonds.

Fig. 1. In (A), chain A (yellow) and chain B (blue) of 4Y87. This is the PDE9 enzyme in complex with its inhibitor, 49E. Protein in ribbon, and ligands in ball and stick mode. The IC$_{50}$ values for two PDE9 inhibitors, (B) 49E and (C) 35, were 11.0 nM and 0.6 nM, respectively.

Fig. 2. Molecular structure of 46 secondary metabolites of *Andrographis paniculate*.

MD simulation

MD simulations were performed on the PDE9-ligand complexes which each initial conformation of the protein-ligand complex was a molecular docking result with the lowest free energy of binding. The protein topology was prepared using MD simulations of protein-ligand complexes were carried out using the Gromacs. The protein topology was generated using the AMBER99SB-ILDN force field (31) while the ligand topology was prepared using the general AMBER force field (GAFF) (32) by the antechamber package with the assistance of ACPYPE.

The initial conformation in the MD simulation is a protein-ligand complex resulting from the molecular docking simulation with the lowest binding energy. Solvation of protein-ligand complex using the water molecule model TIP3P31 in cubic space. The neutral system was obtained after the addition of Na⁺/Cl⁻ ions.

The system (chain A of PDE9, counterions, and ligands) was in equilibrium after NVT and NPT simulations at 299,177 K for 100 ps each. Simulation of the whole system as the target of MD production took place at a temperature of 298.25 K and a pressure of 1 bar for 100 ns. The RMSD and MMPBSA, as well as MMGBSA

for the free energy of binding, were calculated from the MD simulation results using gmx MMPBSA and gmx MMPBSA ana.
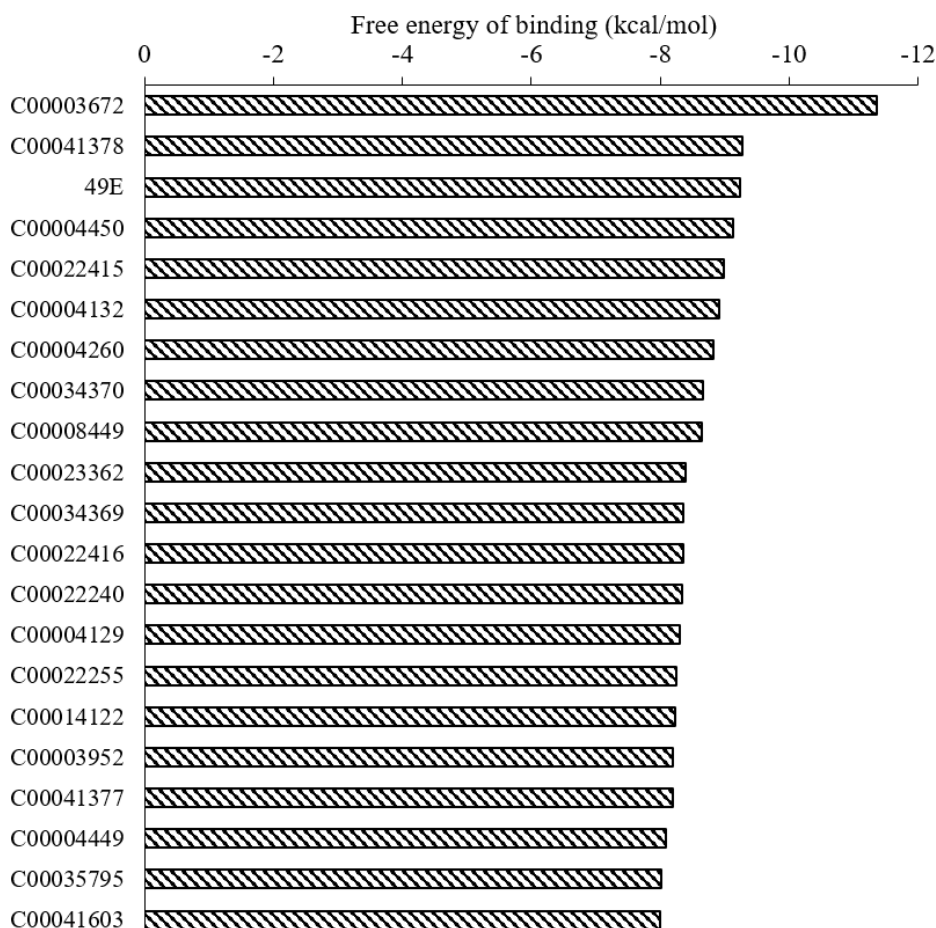
RESULTS

Molecular docking

The PDB code of macromolecule in this study is 4Y87 which are contain PDE9 protein and the 49E compound as a native PDE9 inhibitor. The results of the 49E re-docking showed that the best pose had an RMSD of 1.5676 Å with a binding free energy of -8.26 kcal/mol. The grid box dimension of the validated active site was 47, 31, 31 (the number of grid points in x, y, and z directions), and the spacing is 0.375. The visualization of the native ligands before and after re-docking is shown in Fig. 3A and B. The six amino acid residues of PDE9 that showed interaction with the selected native ligand pose as a redocked result were GLN513 as the H-bond acceptor, ILE463 in the H-bond carbon interaction, and four amino acids showing the ability of hydrophobic interaction with the ligand (Fig. 3B).

The docking results of the test ligands in Fig. 4 showed that 20 compounds had free energy of binding of less than -8.00 kcal/mol.
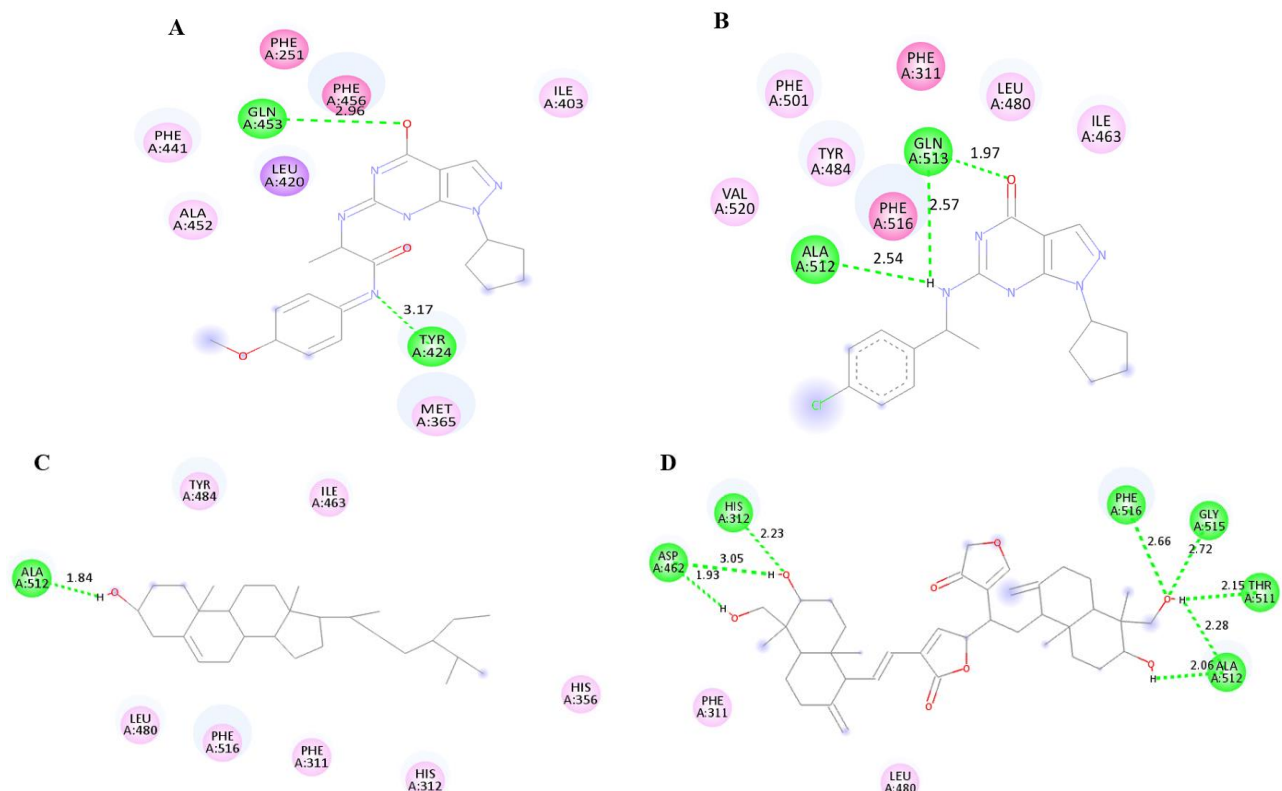
Fig. 3. The interaction of ligands with phosphodiesterase-9. (A) 49E in crystal structure, (B) 49E, (C) C00003672, and (D) C00041378 in selected poses.

Fig. 4. The results of the molecular docking of 21 secondary metabolites of *Andrographis paniculata* with a free energy of binding < -8.00 kcal/mol.
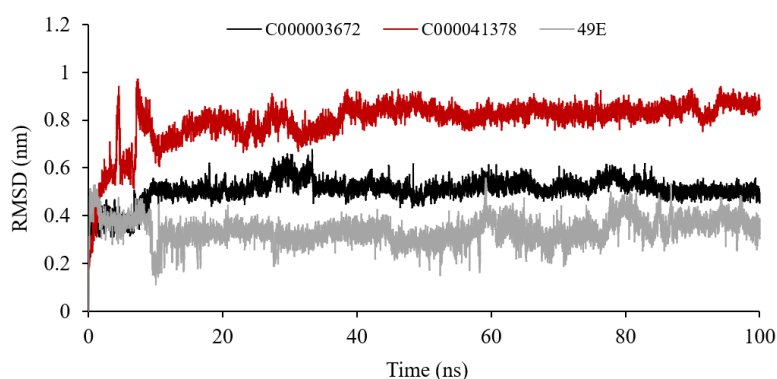
Fig. 5. Root mean square distance of C00003672, C00041378, and 49E throughout the simulation.

Molecular dynamic simulation

The RMSD during the MD simulation of C00003672, C00041378, and 49E (native ligand) is shown in Fig. 5.
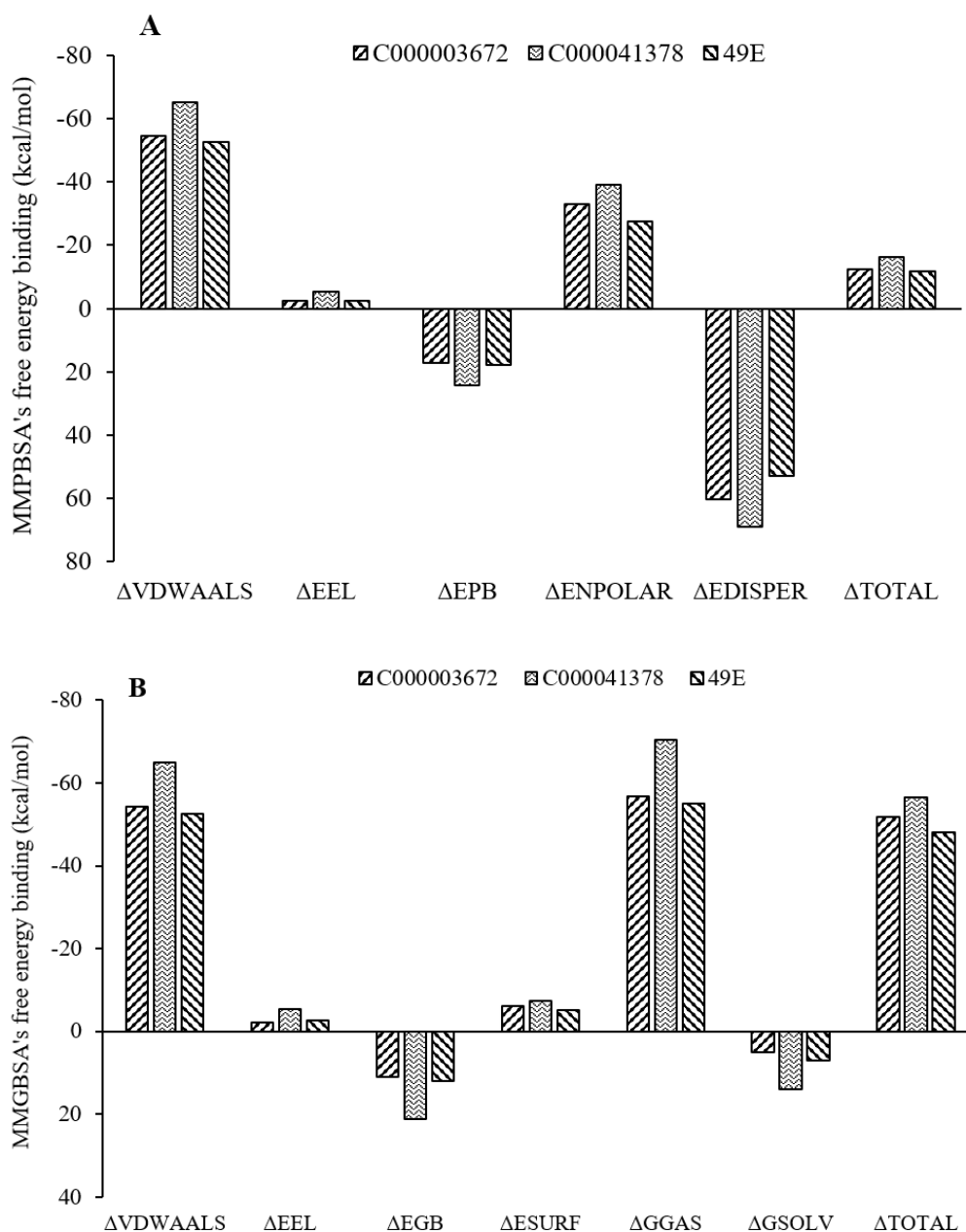
The free energy of binding and the energy decomposition of each ligand are shown in Figs. 6 and 7, respectively. Figure 6 shows that the ΔGMMGBSA of C00003672, C00041378, and 49E were -51.69, -56.43, and -48.13 kcal/mol, respectively, and the ΔGMMPBSA of C00003672, C00041378, and 49E were -12.26, -16.24, and -11.79 kcal/mol, respectively. The number of PDE9 amino acids located at a distance of 5 Å from C00003672 is 25 residues, *i.e.*, PHE311, HIS312, HIS316, HIS352, ASP353, HIS356, ASN360, LEU381, GLU382, HIS385, THR423, MET425, ASP462, ILE463, SER464, ASN465, LEU480,

TYR484, PHE501, THR511, ALA512, GLN513, GLY515, PHE516, and VAL520. The number of PDE9 amino acids located at a distance of 5 Å from C00041378, is 31 residues, i.e., HIS312, HIS316, HIS352, ASP353, HIS356, ASN360, ASN361, LEU381, GLU382, HIS385, THR423, ASP424, MET425, ALA426, HIS428, ALA429, ASP462, ILE463, LEU480, TYR484, PHE501, VAL507, ALA510, THR511, ALA512, GLN513, ILE514, GLY515, PHE516, PHE519, and VAL520. The number of PDE9 amino acids located at a distance of 5 Å from C00003672 is 17 residues, i.e., PHE311, HIS312, MET425, ASP462, ILE463, ASN465, GLU466, VAL477, LEU480, TYR484, PHE501, THR511, ALA512, GLN513, PHE516, VAL520, and LEU521. The decomposition of MMGBSA and MMPBSA's free energy of binding for each binding pocket PDE9 is summarized in Fig. 7.

Fig. 6. Free energy of binding of C00003672, C00041378, and 49E by (A) MMPBSA and (B) MMGBSA calculation in interaction with phosphodiesterase-9.
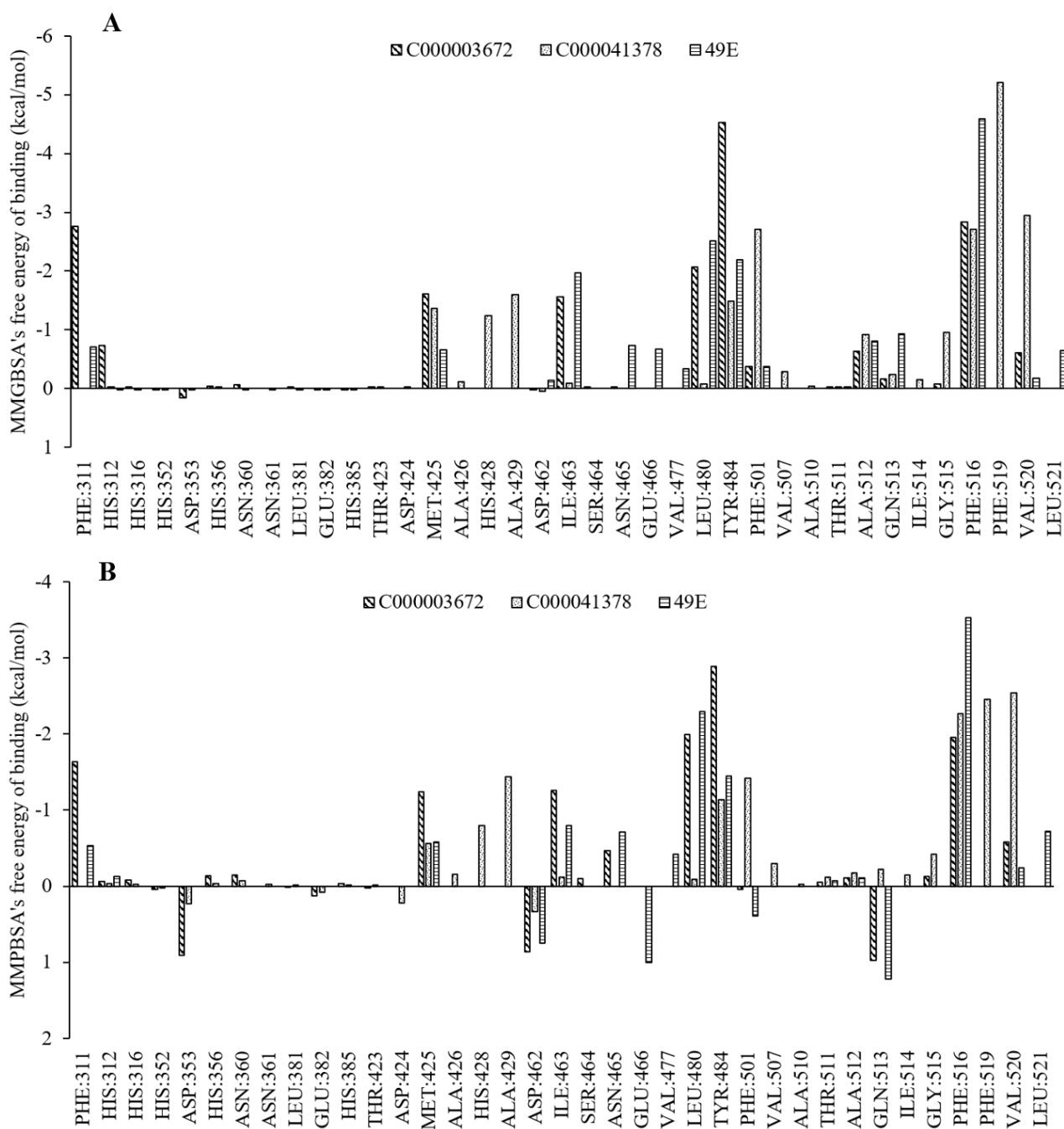
Fig. 7. Decomposition of the (A) MMGBSA and (B) MMPBSA's free energy of binding of C00003672, C00041378 and 49E in interaction with the active site of phosphodiesterase-9.

DISCUSSION

Determination of the target active site is an important step in conducting molecular docking simulations. In many cases, the location of the active site can be determined easily if the target protein is crystallized together with a native ligand (33). The target protein with code 4Y87 is a PDE9 enzyme in complex with 49E as an inhibitor with an IC_{50} of 16 nM (26). The X-ray diffraction crystal structure of the PDE9-49E complex shows the interaction of the ligand with the active site of PDE9 formed by two bonds, namely a hydrogen bond between the O atom of 49E as an acceptor with the NH side chain of GLN513 as a donor, and π-stacking between the pyrazolopyrimidinone ring of 49E and the PHE516 side chain cyclic group (26). If the interaction criteria use the default setting, another hydrophobic interaction involving six amino acids will be seen, such as in Fig. 3A.

The PDE9 binding site was checked by implementing a native ligand re-docking protocol. The coordinates of each atom of the ligand molecule before and after re-docking were compared, and the RMSD was calculated. The results of the 49E re-docking showed that the best pose had an RMSD of 1.5676 Å with the free energy of binding of -8.26 kcal/mol. The pose is obtained at grid settings x, y, z, equal to 46, 30, 30, coordinates of the central grid point of the maps (78.077, 52.956, 42.171), minimum coordinates in the grid (69.452, 47.331, 36.546), and maximum coordinates in the grid (86.702, 58.581, 47.796). The interaction criteria use the default settings of the Discovery Studio Visualizer (23).

The six amino acid residues of PDE9 that showed interaction with the selected native ligand pose as a redocked result were GLN513 as the H-bond acceptor, ILE463 in the H-bond carbon interaction, and four amino acids showing the ability of hydrophobic interaction with the ligand (Fig. 3B). Based on the re-docking RMSD, the negative free energy of binding, and consistency of amino acid residues interacting with the ligand, the PDE9 binding site in the 4Y87 crystal structure is the active site of PDE9.

Molecular docking simulation of each secondary metabolite of AP was carried out by applying the same parameter settings as native ligand re-docking. Two compounds with higher free energies binding than the native ligands are C00003672 and C00041378 with -11.35 and -9.27 kcal/mol, respectively. The free energy of binding of 49E as a native ligand is only -9.23 kcal/mol. Figure 4, a graph of the free energies of binding between PDE9 and ligand shows a summary of the docking results.

In molecular docking, the free energy of binding is the predictive force of ligand and protein interaction. PDE9, as a subtype of PDE, is one of the enzymes that hydrolyze cGMP and cAMP, while cGMP itself is one of the signaling pathways to reduce insulin resistance. The development of anti-diabetic drugs targeted PDE9 as an inhibitor with the assumption that the stronger the ligand-receptor interaction, the greater the ability of the ligand as an inhibitor of the receptor.

The interaction of C00003672 with PDE9 is formed by one hydrogen bond, namely the ligand hydroxyl as donor and OE2 of GLU382 of the enzyme as acceptor, with an interaction distance of 1.94 Å. Other types of ligand-PDE9 interactions include hydrophobic interactions such as phi-sigma, phi-alkyl, and alkyl-alkyl. Ligand C00003672 interacts with 20 amino acid residues of the PDE9 active site, consisting of one hydrogen bond with GLU382 as an acceptor, forming phi-sigma, alkyl-alkyl, and phi-alkyl hydrophobic interactions with seven amino acids, involving van der Waals interactions with 12 amino acids, and steric bumping with the Zn^{2+} and Mg^{2+} metal ions (Fig. 3C). Ligand C00041378 forms a hydrogen interaction with the five amino acids of the active site of PDE9 and a hydrophobic interaction with two amino acids. The Mg^{2+} ion exerts a repulsive force on the ligand (Fig. 3D). Therefore, the docking result showed two secondary metabolites of AP with the free energy of binding resulting from molecular binding have prospects for further study as new anti-diabetic compound candidates that work through PDE9 inhibition.

The two secondary metabolites of AP, C00003672, and C00041378 (which had higher free energy of binding than 49E), were examined for their interaction stability with PDE9 protein by an MD approach. MD simulations were carried out for 50 ns. The RMSD during the simulation of two AP metabolites and one native ligand is shown in Fig. 5. Based on the RMSD value, the movement distance of each compound during the simulation was less than 1.0 nm from the initial position. The smallest movement distance of ligands was the native ligand, then C00003672 and the furthest movement was C00041378.

Confirmation of the interaction stability of each ligand can also be seen in the mean of free energy of binding (Fig. 6) and the energy decomposition calculation (Fig. 7) as the results of the MD simulation. The free energy of binding of each PDE9-ligand complex during the MD simulations was calculated by applying the MMGBSA or ΔGMMGBSA and the MMPBSA or ΔGMMPBSA. The residue' contribution was calculated by using the energy

decomposition feature of gmx_MMPBSA by applying the MMGBSA and MMPBSA methods. ΔGMMGBSA and ΔGMMPBSA are the sums of the free energy in the gas phase (ΔG gas) and the free energy in the dissolved phase (ΔG Solv). ΔG gas is the energy obtained from the sum of the bonding and non-bonding energy. Bonding energy consists of bond, angle, and dihedral energy, and non-bonding energy is contributed by van der Waals energy and electronic energy. In ΔGMMGBSA calculation, ΔG Solv is the sum of generalized born energy and surface area energy, while in ΔGMMPBSA calculation, ΔG Solv is contributed by Poisson-Boltzmann energy, non-polar solvation energy, and dispersion energy. Generalized born energy and Poisson-Boltzmann energy are polar energy, and the others are non-polar energy. Free energy of binding in PDE9 interactions with C00003672, C00041378, and 49E ligands are -51.69, -56.43, and -48.13 kcal/mol, respectively for MMGBSA, and -12.26, -16.24, and -11.79 kcal/mol, respectively for MMPBSA method. The free energy of binding, which plays a role in the PDE9-ligand interaction and is depicted in Fig. 7, was determined based on the findings of an investigation of the residual energy. The free energy of binding, which plays a role in the PDE9-ligand interaction and is depicted in Fig. 7, was determined based on the findings of an investigation of the residual energy. The free energy of binding, which plays a role in the PDE9-ligand interaction and is depicted in Fig. 7, was determined based on the findings of an investigation of the residual energy. Only PHE311 (-2.76 kcal/mol), MET425 (-1.61), ILE463 (-1.56), LEU480 (-2.06), TYR484 (-4.53), and PHE516 (-2.84) have bonding strengths lower than -1.0 kcal/mol among the 25 amino acids that make up the binding pocket of PDE9 in interaction with C00003672 (blue). Only PHE311 (-2.76 kcal/mol), MET425 (-1.61), ILE463 (-1.56), LEU480 (-2.06), TYR484 (-4.53), and PHE516 (-2.84) have bonding strengths lower than -1.0 kcal/mol among the 25 amino acids that make up the binding pocket of PDE9 in interaction with C00003672. Only MET425 (-1.36), HIS428 (-1.24), ALA429 (-1.60), TYR484 (-1.49), PHE501 (-2.71), PHE516 (-2.71), PHE519

(-5.20), and VAL520 (-2.95) have bonding strengths lower than -1.0 kcal/mol among the 31 amino acids that make up the binding pocket of PDE9 in interaction with C000041378 (orange). Only MET425 (-1.36), HIS428 (-1.24), ALA429 (-1.60), TYR484 (-1.49), PHE501 (-2.71), PHE516 (-2.71), PHE519 (-5.20), and VAL520 (-2.95) have bonding strengths lower than -1.0 kcal/mol among the 17 amino acids that make up the binding pocket of PDE9 in interaction with 49E (grey).

In the interaction with the PDE9 active site, C00041378 showed consistency and similarity with 49E, but the main contribution was shown by their interaction with PHE516. Based on the MMGBSA and MMPBSA energy calculation, the native ligand (49E) has a free energy of binding lower than the two AP secondary metabolites, C00003672 and C00041378. However, C00041378 showed ability as a PDE9 inhibitor because, apart from having free energy of binding close to 49E, the ligand also showed a tendency to interact with similar residues that are shown by 49E, namely TRY484. The C00041378 also demonstrates that it interacts with PDE9 *via* the PHE516 residue, which contributes significantly to the free energy of binding. The interaction of PDE9 inhibitors with PHE516 residues was also shown by other PDE inhibitors, namely compound 35O (3r). This compound has been proven to inhibit PDE9 with an IC_{50} of 0.6 nM (27). Therefore, C00041378 as an AP secondary metabolite is a potential compound for antidiabetic agents.

CONCLUSION

Based on docking and MD simulation results, it is suggested that one of 46 compounds, namely C00041378 has the potential to be an anti-diabetes candidate by inhibiting PDE9.

Conflict of interest statement

The authors declared no conflicts of interest in this study.

Authors' contribution

N. Ischak, L.O. Aman, and A. Asnawi contributed to the study concept and design, supervised the study, and drafted the manuscript; L.O. Aman and H. Hasan acquired the data; L.O. Aman and A.L. Kilo analyzed and interpreted the data; N. Ischak, L.O. Aman, and A. Asnawi revised the manuscript critically for important intellectual content. The final version of the manuscript was approved by all authors.

REFERENCES

1. IDF Diabetes Atlas. 10th ed. 2022. Available from: https://diabetesatlas.org/
2. Melmed S, Auchus RJ, Goldfine AB, Koenig R, Rosen CJ. Williams Textbook of Endocrinology. 14th ed. Philadelphia, U.S.: Elsevier; 2019. pp. 222-223.
3. Centers for Disease Control and Prevention. National Diabetes Fact Sheet: national estimates and general information on diabetes and prediabetes in the United States, 2011. Atlanta, GA: U.S. Department of Health and Human Services, Centers for Disease Control and Prevention, 2011. Available from: https://web.archive.org/web/20140417143052/http://diabetes.niddk.nih.gov/dm/pubs/statistics/#Gestational.
4. Krentz AJ, Bailey CJ. Oral antidiabetic agents: current role in type 2 diabetes mellitus. Drugs. 2005;65(3):385-411.
   DOI: 10.2165/00003495-200565030-00005.
5. Kleinberger JW, Pollin TI. Personalized medicine in diabetes mellitus: current opportunities and future prospects. Ann N Y Acad Sci. 2015;1346(1):45-56.
   DOI: 10.1111/nyas.12757.
6. Newman DJ, Cragg GM. Natural products as sources of new drugs from 1981 to 2014. J Nat Prod. 2016;79(3):629-661.
   DOI: 10.1021/acs.jnatprod.5b01055.
7. Turner LW, Nartey D, Stafford RS, Singh S, Alexander GC. Ambulatory treatment of type 2 diabetes in the U.S., 1997-2012. Diabetes Care. 2014;37(4):985-992.
   DOI: 10.2337/DC13-2097.
8. Komalasari T, Harimurti S. A Review on the anti-diabetic activity of *Andrographis paniculata* (Burm. f.) Nees based *in-vivo* study. Int J Public Heal Sci. 2015;4(4):256-263.
   DOI: 10.11591/ijphs.v4i4.4743.
9. Nugroho AE, Andrie M, Warditiani NK, Siswanto E, Pramono S, Lukitaningsih E. Antidiabetic and antihiperlipidemic effect of *Andrographis paniculata* (Burm. f.) Nees and andrographolide in high-fructose-fat-fed rats. Indian J Pharmacol. 2012;44(3):377-381.
   DOI: 10.4103/0253-7613.96343.
10. Ischak NI, Botutihe DN. Preliminary study of clinical antidiabetic activity of salam leaves (*Eugenia polyantha*) and sambiloto leaves (*Andrographis paniculata*) in type 2 diabetic patients. IOP Conf Ser Earth Environ Sci. 2020;589(1):1-7.
    DOI: 10.1088/1755-1315/589/1/012034.
11. Akhtar MT, Bin Mohd Sarib MS, Ismail IS, Abas F, Ismail A, Lajis NH, *et al*. Anti-diabetic activity and metabolic changes induced by *Andrographis paniculata* plant extract in obese diabetic rats. Molecules. 2016;21(8):1026,1-18.
    DOI: 10.3390/molecules21081026.
12. Huang YY, Yu YF, Zhang C, Chen Y, Zhou Q, Li Z, *et al*. Validation of phosphodiesterase-10 as a novel target for pulmonary arterial hypertension via highly selective and subnanomolar inhibitors. J Med Chem. 2019;62(7):3707-3721.
    DOI: 10.1021/acs.jmedchem.9b00224.
13. O'Neill JS, Maywood ES, Chesham JE, Takahashi JS, Hastings MH. cAMP-dependent signaling as a core component of the mammalian circadian pacemaker. Science. 2008;320(5878):949-453.
    DOI: 10.1126/science.1152506.
14. Li Z, Huang Y, Wu Y, Chen J, Wu D, Zhan CG, *et al*. Absolute binding free energy calculation and design of a subnanomolar inhibitor of phosphodiesterase-10. J Med Chem. 2019;62(4):2099-2111.
    DOI: 10.1021/acs.jmedchem.8b01763.
15. Ribaudo G, Memo M, Gianoncelli A. A perspective on natural and nature-inspired small molecules targeting phosphodiesterase 9 (PDE9): chances and challenges against neurodegeneration. Pharmaceuticals (Basel). 2021;14(1):58,1-13.
    DOI: 10.3390/PH14010058.
16. Zoete V, Grosdidier A, Michielin O. Docking, virtual high throughput screening and *in silico* fragment-based drug design. J Cell Mol Med. 2009;13(2):238-248.
    DOI: 10.1111/j.1582-4934.2008.00665.x.
17. El-Hachem N, Haibe-Kains B, Khalil A, Kobeissy FH, Nemer G. AutoDock and AutoDockTools for protein-ligand docking: beta-site amyloid precursor protein cleaving enzyme 1(BACE1) as a case study. Methods Mol Biol. 2017;1598:391-403.
    DOI: 10.1007/978-1-4939-6952-4_20.
18. Van Der Spoel D, Lindahl E, Hess B, Groenhof G, Mark AE, Berendsen HJC. GROMACS: fast, flexible, and free. J Comput Chem. 2005;26(16):1701-1718.
    DOI: 10.1002/jcc.20291.
19. Sousa Da Silva AW, Vranken WF. ACPYPE - AnteChamber PYthon Parser interfacE. BMC Res Notes. 2012;5(1):367,1-8.
    DOI: 10.1186/1756-0500-5-367.
20. Pettersen EF, Goddard TD, Huang CC, Couch GS, Greenblatt DM, Meng EC, *et al*. UCSF Chimera-a visualization system for exploratory research and analysis. J Comput Chem. 2004;25(13):1605-1612.
    DOI: 10.1002/JCC.20084.

21. Webb B, Sali A. Comparative protein structure modeling using MODELLER. Curr Protoc Bioinformatics. 2016;54:5.6.1-5.6.37. DOI: 10.1002/cpbi.3

22. AmberTools21. Available from: https://ambermd.org/AmberTools.php.

23. Visualization - BIOVIA - Dassault Systèmes®. Available from: https://www.3ds.com/products-services/biovia/products/molecular-modeling-simulation/biovia-discovery-studio/visualization/

24. ChemAxon. Marvin Sketch. Available from: https://www.chemaxon.com/products/marvin/.

25. Valdés-Tresanco MS, Valdés-Tresanco ME, Valiente PA, Moreno E. gmx_MMPBSA: a new tool to perform end-state free energy calculations with GROMACS. J Chem Theory Comput. 2021;17(10):6281-6291. DOI: 10.1021/acs.jctc.1c00645.

26. Huang M, Shao Y, Hou J, Cui W, Liang B, Huang Y, *et al*. Structural asymmetry of phosphodiesterase-9A and a unique pocket for selective binding of a potent enantiomeric inhibitor. Mol Pharmacol. 2015;88(5):836-845. DOI: 10.1124/mol.115.099747.

27. Shao YX, Huang M, Cui W, Feng LJ, Wu Y, Cai Y, *et al*. Discovery of a phosphodiesterase 9A inhibitor as a potential hypoglycemic agent. J Med Chem. 2014;57(24):10304-10313.

DOI: 10.1021/jm500836h.

28. RCSB PDB - 4Y87: Crystal structure of phosphodiesterase 9 in complex with (R)-C33 (6-{[(1R)-1-(4-chlorophenyl)ethyl]amino}-1-cyclopentyl-1,5-dihydro-4H-pyrazolo[3,4-d]pyrimidin-4-one). 2022. Available from: https://www.rcsb.org/structure/4Y87.

29. KNApSAcK-3D. 2022. Available from: http://knapsack3d.sakura.ne.jp/index.html.

30. Cole JC, Murray CW, Nissink JWM, Taylor RD, Taylor R. Comparing protein-ligand docking programs is difficult. Proteins. 2005;60(3):325-332. DOI: 10.1002/prot.20497.

31. Lindorff-Larsen K, Piana S, Palmo K, Maragakis P, Klepeis JL, Dror RO, *et al*. Improved side-chain torsion potentials for the Amber ff99SB protein force field. Proteins. 2010;78(8):1950-1958. DOI: 10.1002/prot.22711.

32. Wang J, Wolf RM, Caldwell JW, Kollman PA, Case DA. Development and testing of a general amber force field. J Comput Chem. 2004;25(9):1157-1174. DOI: 10.1002/jcc.20035.

33. Meng XY, Zhang HX, Mezei M, Cui M. Molecular docking: a powerful approach for structure-based drug discovery. Curr Comput Aided Drug Des. 2011;7(2):146-157.

DOI: 10.2174/157340911795677602.